CONFIDENTIAL

FINAL PROJECT REPORT
NUMERICAL ASSESSMENT OF SWIMSUITS PERFORMANCE

Partnership:

1) ARENA© Italia S.p.A., Contrada Cisterna 84/85, 62029 Tolentino (MC), Italy

2) MOX - Dept. of Mathematics, Politecnico di Milano, P.zza L. da Vinci 32, 20133 Milano, Italy

A. Veneziani, E. Foa, A. Quarteroni
MOX

SUMMARY

1 INTRODUCTION

This is the Final Report for the Project *Numerical Assessment of Performances of Swimsuits*, developed in the framework of the Partenrship between Arena and MOX. The Project (see [11]) had the aim of the numerical study of specific features of new swimsuits for Athens 2004 Olympic Games.

The Project was finalized to two goals:

1. Water dynamics investigations: in the development of the new swimsuit after Powerskin©, namely PowerSkin Xtreme©, numerical simulations were intended to give some insights in the identification of possible high drag zones on a swimmer body during a competion and to investigate new tissue solutions. Some roughness of the swimsuit surface induced by the presence of the fibers could introduce in the turbulent water dynamics a *riblets* effect, yielding a drag reduction during a competition. Numerical simulations were intended to support the investigations on this effect.

2. Advertising: Numerical simulations were intended to provide impressive images supporting the advertising of the new product.

The project was split into two tasks.

1. *Microscopic simulations*: numerical simulations at the space scale of a few tissue fibers in order to understand possible effects of roughness induced by the fibers.

2. *Macroscopic simulations*: numerical simulations at the space scale of a swimmer in order to investigate possible parts of the body featuring high shear stresses and the overall effects of new tissues.

This is the second and final Report planned for this Project. The Mid Term Report [12] described the development of the Project from the kick-off (December 15^{th} 2003 to the end of April, 2004). In this Final Report we start from the results yielded at the end of April [12] and describe the new results and simulations, giving conclusions and possible future developments.

1.1 State of the Art after the first Report

After the first part of the Project we obtained the following results:

Micro-analysis A pipeline for the simulation of the tissue fibers at the microscale was established, by setting up ad hoc codes for the fibers geometrical virtual construction and meshing. Some preliminar simulations were performed. We planned more simulations on the microscopic scale in order to compare the new tissue used in PowerSkin Xtreme© with the one adopted for PowerSkin©.

Macro-analysis A first geometrical reconstruction of a swimmer was obtained starting from data files delivered by TELMAT (see [12]). Numerical simulations performed on this geometry have shown that on the swimmer body there are some critical high shear stresses zones. Interestingly enough, these zones corresonded to part where special tissue was applied in PowerSkin Xtreme©.

Finally, we came to the following conclusions:

1. Geometrical recontructions should be improved. Actually, the filterig of the original noisy data coming from TELMAT (see [12]) seemed too strong, in particular in the region round the swimmer's head. A more refined geometrical reconstruction seemed to be mandatory.

2. A strict coordination with the group performing experimental measures was recommended for obtaining precise values for parameters used in the macroscopic simulations.

In the next Sections we describe the continuation of the two Tasks of the Project.

2 MACROSCOPIC NUMERICAL INVESTIGATIONS

After the acquisition of the data of Emiliano Brembilla's body, obtained with the SYMCAD©device of TELMAT, we subdivided the Task of Macroscopic Numerical Investigations into three steps:

1. Geometrical reconstruction

2. Meshing

3. Simulations

In [12] we obtained some numerical simulations on a first reconstructed geometry. Even if numerical results were quite good at a qualitative level, we decided to improve the geometrical reconstruction in order to have more accurate simulations. Here, we describe the steps carried out for this aim and the new numerical results obtained.

2.1 Geometrical reconstruction of a Swimmer Body

In [12] we illustrated the steps and the difficulties we faced for the geometrical reconstruction of Emiliano Brembilla into CAD codes. Original data delivered by TELMAT were split into two parts (upper and lower body) and were very noisy. We resorted to some filetered file obtained by TELMAT software. By so doing, we obtained a first reconstruction with some simplifications due to the effects of filtering in some parts of the body (the head in particular). In order to improve the geometrical reconstruction, we decided to resort to the non filetered file and to proceed following the Flow Chart of Fig. 1. In particular, we performed a first manual filtering. Then we extracted the normal (i.e. saggital) sections of Brembilla's body (like in [12]) and then we finally smoothened the reconstructed geometry, as we are going to describe.

2.1.1 Improvements in the Geometry Reconstruction

As for the first geometrical reconstruction, the steps for obtaining the swimmer's body surface have been:

1. Normal (saggital) sections extraction

2. Spline interpolation of each section

3. Surface fitting

As previously pointed out this time the steps have been perfomred on the complete (non fileterd) data file and the noise filtering and the smoothing has

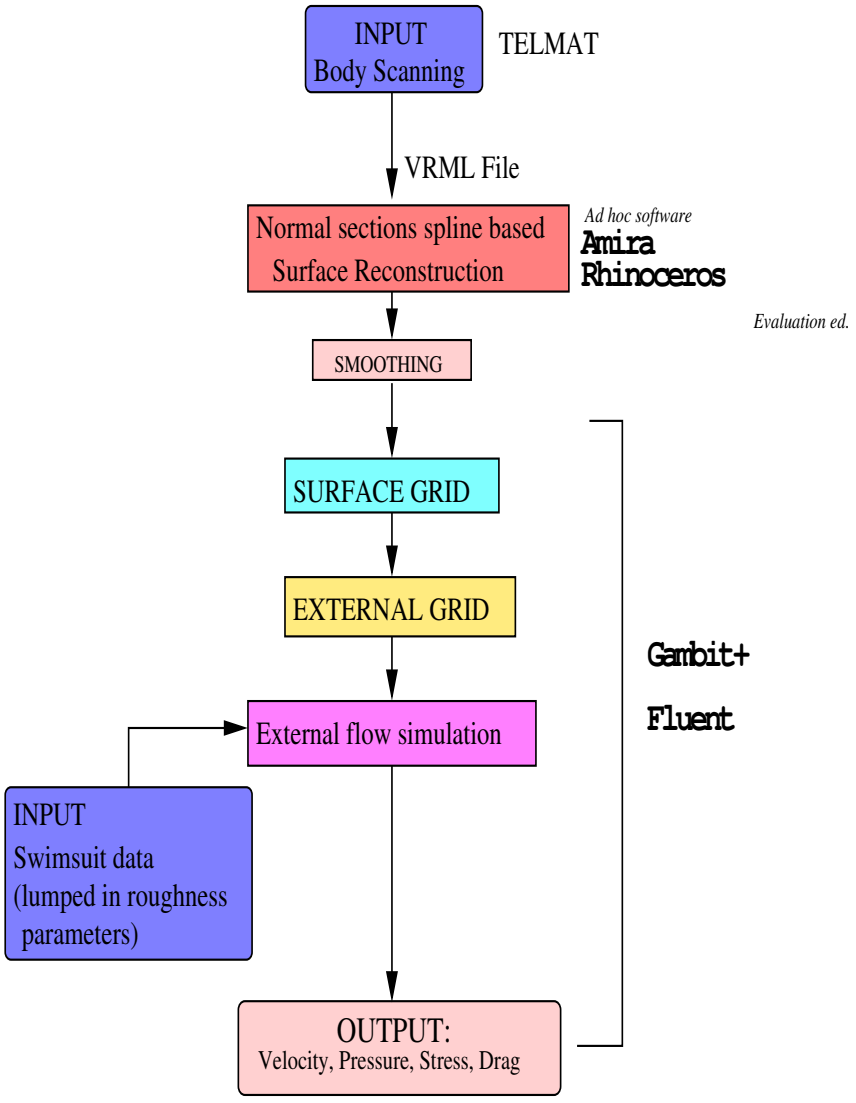

Figure 1: Flow chart of the steps for the *macroscopic* simulations.

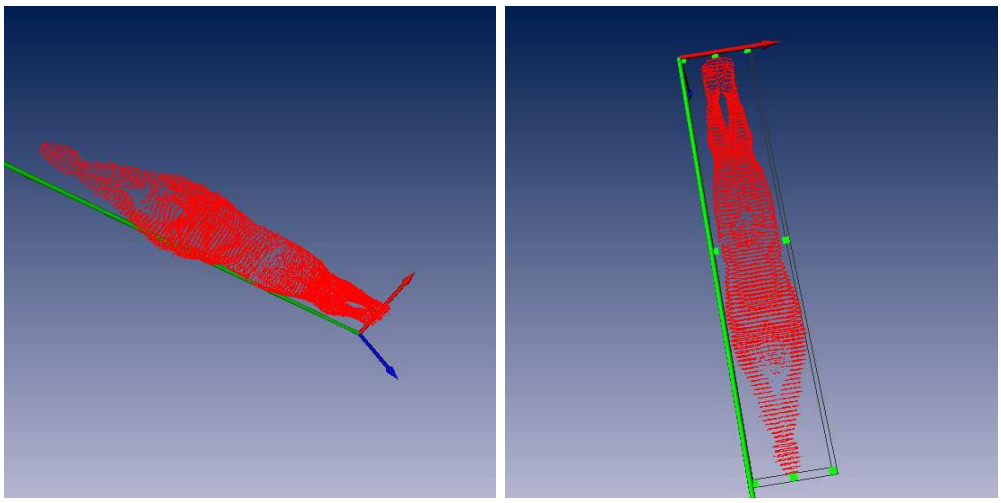

Figure 2: Axial sections obtained with an "ad hoc" code and represented in AMIRA.

been performed after the surface fitting. We used `Gambit`, the pre-processor module of Fluent. In particular, in the first geometry we used for the numerical simulations the arms and the legs of the swimmer were joined (see [12]). This was supposed to affect the numerical simulations in a significant way and it was a drawback of the data filtering performed by Telmat; actually, the software used for the surface fitting, AMIRA (see Fig. 2), was unable to find the holes between the legs and the arms in building the surface reconstruction.

So we decided to proceed with the original complete file. We started again by building an uncorrect surface and in a second stage we introduced the holes. More precisely:

1. from the original TELMAT file with the points cloud we extract 140 normal sections. A "ad hoc" code has been used. The number 140 is the result of several trials for identifying the good compromise between the need of an accurate reconstruction and low computational costs;

2. each section has been interpolated by splines (see Fig.3)

3. the 140 interpolated sections have been linked in one file (see Fig.4) and a surface covering all the sections has been computed (see Fig.5)

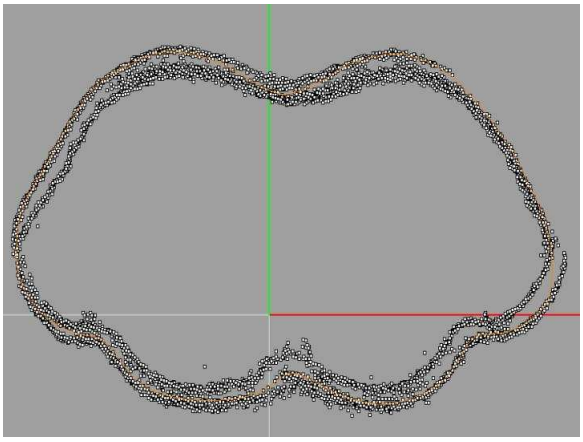

Figure 3: One normal section with its interpolating spline.

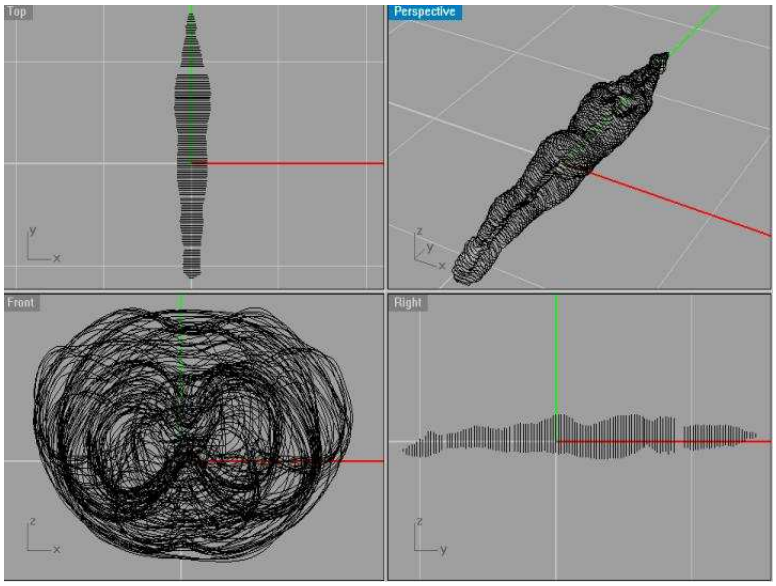

Figure 4: Curve reconstruction.

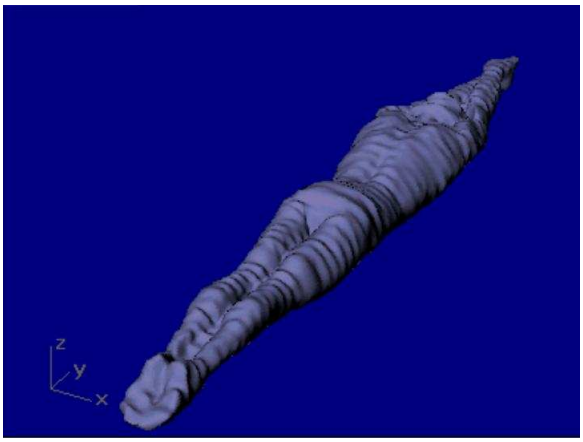

Figure 5: Pre-smoothing geometry.

4. Some manual correction has been introduced with smoothing operation for improving the reconstructed geometry. The geometry still featured joined arms and legs (see Fig.6).

5. The holes between the arms and between the legs have been introduced *after* this reconstruction. Actually, all the temptatives of building directly a reconstruction with more than one normal section at the same level (corresponding to the two legs, or the two arms or the two arms with the head) failed due to problems in the surface fitting; The holes have been obtained by working in `Gambit`, subtracting suitable geometries to the reconstructed body. The result is shown in Fig. 7.

A comparison between Fig. 5 and Fig. 6 allows to appreciate the effect of smoothing. Fig. 7 outlines the presence of the holes.

2.2 Mesh generation. Sensitivity analysis

The grid has been generated with `Gambit` (licence has been acquired by Arena from the end of May 2004, following the recommendation in [12]. Starting from the files obtained by `Amira` and `Rhinoceros` (evaluation version), some topological corrections have been required in order to have a meshable surface.

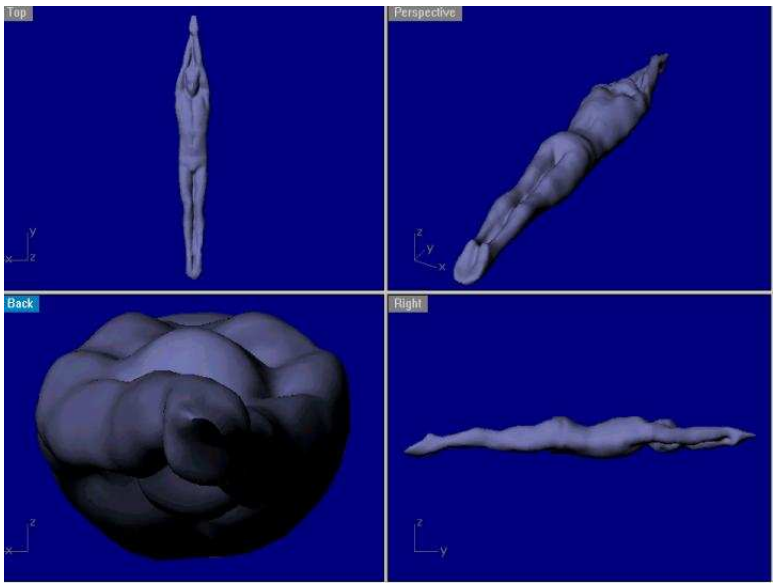

Figure 6: Post-smoothing geometry.

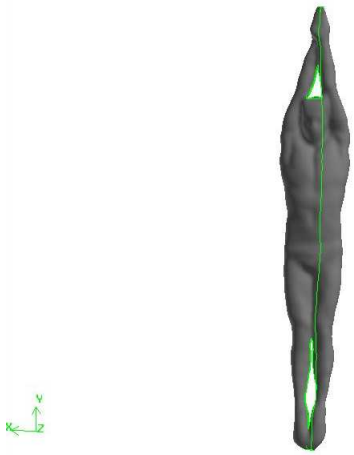

Figure 7: Geometry reconstruction with holes between the arms and the legs.

The swimmer has been immersed in a water domain that has been assumed to be cylindrical. This shape allows some simplification in the prescription of the boundary conditions for the numerical simulation. The computational domain has been obtained by subtraction of the swimmer body to the cylinder. It is worth mentioning that the external boundaries of the cylinder are assumed to be significantly far away from the body of the swimmer. In fact, the diameter of the cylinder was $6m$ and the height was $12m$. In this way the prescription of an inlet velocity profile matching a given flow rate does not significantly affect the velocity field around the swimmer.

The volume grid needed for fluid dynamics numerical simulations can be tipically of two kinds:

1. *tethraedrical*

2. *prismatic.*

Smaller are the elements (tethraedrical or prismatic) and more accurate are the numerical results of the computation (see for example [4]), even if simulation becomes more expensive in terms of CPU times. The main difficulties in the set up of the computational grid is to find the right comprimise between the need of a grid fine enough and the need of reducing computational costs. Tipically, the mesh should be built up in such a way that it is very fine in the region of interest (around the swimmer in our case) and coarse in the other parts of the domain. Tethraedrical elements are very versatile so these meshes are well suited for complex geometries with elements very fine in some parts of the domain and coarse in the other parts. On the other hand, prismatic meshes are better controlled in terms of dimensions (that means controlling the accuracy of the solution). When working on the geometry *without* the holes we decided to use a *mixed* mesh. The grid is tetrahedrical in the whole domain apart a small layer around the swimmer surface (*boundary layer*). In such a way, the grid (and the solution) in the region of interest is under control for capturing the relevant scales around the swimmer (see Fig. 8).

Unfortunately, when resorting to the geometry featuring the holes, `Gambit` was unable to generate a mixed grid due to the topological complexity of the domain. We resorted therefore to fully tetrahedrical meshes. For a better control of the mesh dimensions, two regions has been introduced, a smaller volume around the swimmer with a fine grid and an external coarse subdomain (Fig. 9).

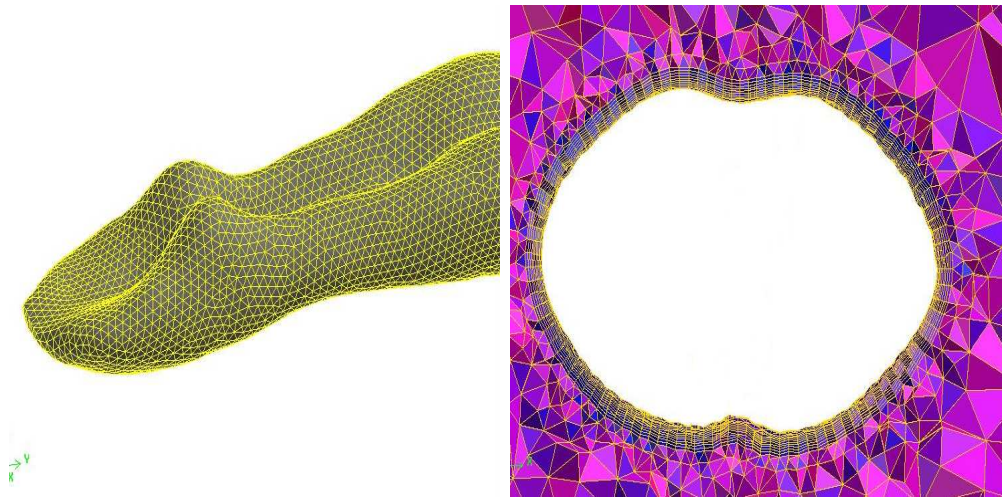

Figure 8: Example of the surface grid over the swimmer (left) in a mesh with a prismatic elements boundary layer. On the right, a normal section around the thorax, putting in evidence the boundary layer.

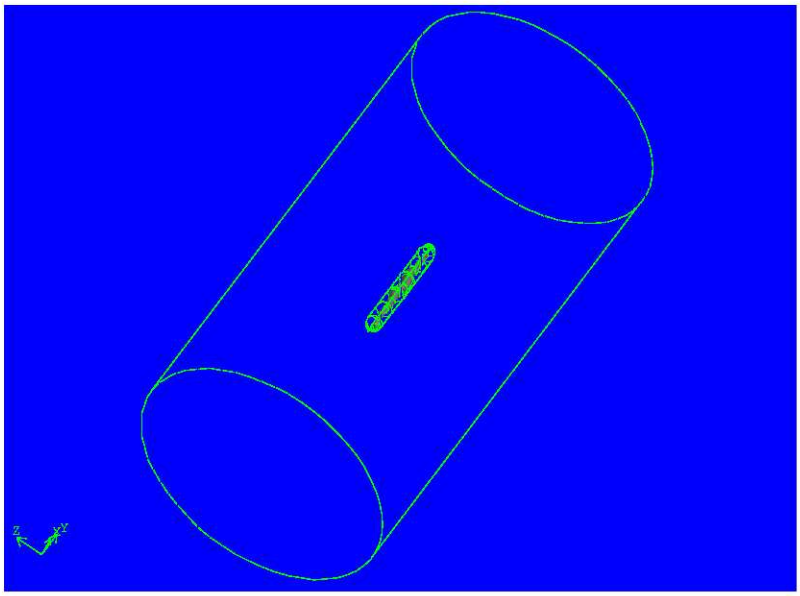

Figure 9: Subdomain region around the swimmer for purely tetrahedrical mesh.

We performed some preliminar numerical simulations in order to understand the role of geometrical simplifications and of the mesh. We set up two meshes with boundary layer and two fully tetrahedrical meshes:

without prismatic boundary layer

1. coarse mesh (denoted by L1) with:
   - mesh size on the swimmer surface: $0.01m$
   - mesh size on the interface between fine and coarse region: $0.02m$;
   - mesh size on the external cylindrical surface: $0.5m$.
2. fine mesh (denoted by NORM) with:
   - mesh size on the swimmer surface: $0.005m$
   - mesh size on the interface between fine and coarse region: $0.02m$;
   - mesh size on the external cylindrical surface: $0.5m$.

with boundary layer

1. coarse mesh (denoted by BL1) with:
   - mesh size on the swimmer surface: $0.01m$
   - height of the first layer of cells: $h = 0.001m$;
   - growing ratio in the boundary layer[1]: $g = 1.1$
   - number of cell layers in the boundary layer: $n = 10$
   - total height of the layer:

$$h(1 + g + g^2 + \ldots + g^n) = h\frac{g^{n+1} - 1}{g - 1} = 0.0159m$$

   - mesh size on the external cylindrical surface: $0.5m$.
2. fine mesh (denoted by BL3) with:
   - mesh size on the swimmer surface: $0.007m$
   - height of the first layer of cells: $h = 0.0005m$;

[1]the growing ratio is the ratio between the dimensions of two consecutive cells moving away from the swimmer's surface.

- growing ratio in the boundary layer: $g = 1.2$
- number of cell layers in the boundary layer: $n = 10$
- total height of the layer: $0.012m$.
- mesh size on the external cylindrical surface: $0.5m$.

The fluid in the computational domain is *Water* with density $\rho = 998.20001kg/m^3$ and viscosity $\nu = 0.001003kg/(ms)$.

In the simulations, we adopted a frame of reference moving with the swimmer (at a constant velocity). Therefore, the swimmer is assumed to be at rest and the water is moving. The boundary conditions adopted for the simulations are:

1. *swimmer body*: velocity $\mathbf{u} = \mathbf{0}$;

2. *inlet*: upwind circular section of the cylinder, where the water is incoming with a constant velocity of $2m/s$.

3. *outlet*: downwind circular section of the cylinder, where the water is outoing. The usual boundary conditions for outlet sections are:

$$p\mathbf{n} - \nu\nabla\mathbf{u} = \mathbf{0}.$$

4. *external surface*, given by the lateral surface of the cylinder, with conditions simulating the presence of the water uniform around the cylinder, where zero normal velocity and zero normal gradients of all the variables are prescribed.

If we assume a characteristic velocity of $2m/s$ and a characteristic length of $1.80m$, the Reynolds number is:

$$Re = \frac{\rho u L}{\nu} = \frac{998.20001 \times 2 \times 1.8}{0.001003} \approx 10^6.$$

The turbulence has been modelled with a $k - \epsilon$ model (see f.i. [3]), so that besides velcity and pressure fields, two more equations are solved, the turbulent kinetic energy k and its rate of dissipation ϵ. In the turbulent boundary layer (where the viscous effects are relevant) suitable wall functions coded in Fluent are adopted.

For the results analysis, we considered:

- velocity magnitude(Fig. 12)
- axial velocity
- static and totale pressure
- wall shear stresses (Fig. 12)

and integral value on the swimmer surface:

- axial total force (DRAG)
- vertical total force (LIFT).

Sensitivity Analysis In Tab. 1, 2, 3 we illustrate the results obtained in order understand if the computational meshes adopted were fine enough and at which extent the geometrical improvements affect the numerical results.

More precisely, the following tables illustrate:

1. comparison among four meshes (two with boundary layer, two without) for the geometry without holes (Tab. 1);
2. comparison between two meshes (without boundary layer) for the geometry with holes (Tab. 2);
3. comparison between the cases with and without holes for the two meshes without boundary layer (Tab. 3).

From the analysis of these results, we can draw the following conclusions.

1. The examination of Table 1 suggests that, apart the coarse mesh without boundary layer, numerical results are quite similar. In particular, observe that the drag and lift results are comparable and weakly dependent on the adopted meshes. This means that the adopted meshes are fine enough for the computations.
2. Tab. 2 leads to similar conclusion for the case with holes (only tetrahedrical meshes): drag results are almost independent of the grid.
3. For what concerns the presence of holes (Tab 3), as it was to be expected it affects essentially the lift computation and the drag is increased up to 10%. We therefore conclude that *the presence of the holes cannot be neglected* in a quantitative numerical assessment of the swimsuit.

	L1	**NORM**	**BL1**	**BL3**
CPU Time	7h 50min	23h 15min	7h 40min	18h 50min
$h_{swimmer}$	0.01	0.005	0.01	0.007
h_{layer}	0.02	0.02	0.001,1.1,10	0.0005,1.2,10
h_{ext}	0.5	0.5	0.5	0.5
$\|\|\mathbf{u}\|\|$ [m/s]	0→2.53	0→2.6897	0→2.7116	0→2.7874
u_y [m/s]	-2.51→0.59	-2.6564→0.5882	-2.67→0.7486	-2.75→0.7840
wss [Pa]	0→20.19	0→25.58	0→25.66	0→28.95
p_{sta} [Pa]	-2212.1→1925.5	-2538.7→2108.1	-2391.7→2108.1	-2597.5→2037.2
p_{dyn} [Pa]	0.79→3376.3	0.22→3689.6	0.22→3671.6	0.07→3878.7
p_{tot} [Pa]	-393.3→2854.4	-403.6→2385.5	-398.6→2360.12	-647.5→2780.9
F_x [N]	2.68	-3.99	-2.46	-2.53
F_y [N] **(drag)**	-45.76	-45.18	-45.35	-44.95
F_z [N] **(lift)**	15.08	16.44	17.15	16.93

Table 1: Numerical results for the geometry without holes with different meshes.

	L1	**NORM**
CPU Time	8h 15min	23h 35min
$h_{swimmer}$	0.01	0.005
h_{layer}	0.02	0.02
h_{ext}	0.5	0.5
$\|\|\mathbf{u}\|\|$ [m/s]	0→2.5347	0→2.6904
u_y [m/s]	-2.4717→0.3	-2.664→0.4701
wss [Pa]	0→21.36	0→24.95
p_{sta} [Pa]	-2312.4→1806.8	-2565.0→2122.6
p_{dyn} [Pa]	0.36→3515.1	0.6 →3640.2
p_{tot} [Pa]	-667.3→2189.8	-932.8→2382.7
F_x [N]	-3.39	-4.06
F_y [N] **(drag)**	-48.88	-48.58
F_z [N] **(lift)**	7.81	7.74

Table 2: Numerical results for the geometry with holes with different meshes.

	Without Holes	Holes
CPU Time	23h 15min	23h 35min
$h_{swimmer}$	0.005	0.005
h_{layer}	0.02	0.02
h_{ext}	0.5	0.5
N_{elem}	1333018	1344890
$\|\|\mathbf{u}\|\|$ [m/s]	0→2.6897	0→2.6904
u_y [m/s]	-2.6564→0.5882	-2.664→0.4701
wss [Pa]	0→25.58	0→24.95
p_{sta} [Pa]	-2538.7→2108.1	-2565.0→2122.6
p_{dyn} [Pa]	0.22→3689.6	0.6 →3640.2
p_{tot} [Pa]	-403.6→2385.5	-932.8→2382.7
F_x [N]	-3.39	-4.06
F_y [N] **(drag)**	-45.18	-48.58
F_z [N] **(lift)**	16.44	7.74

Table 3: Numerical results for the geometries without and with holes on a mesh with similar features. Comparison of the results.

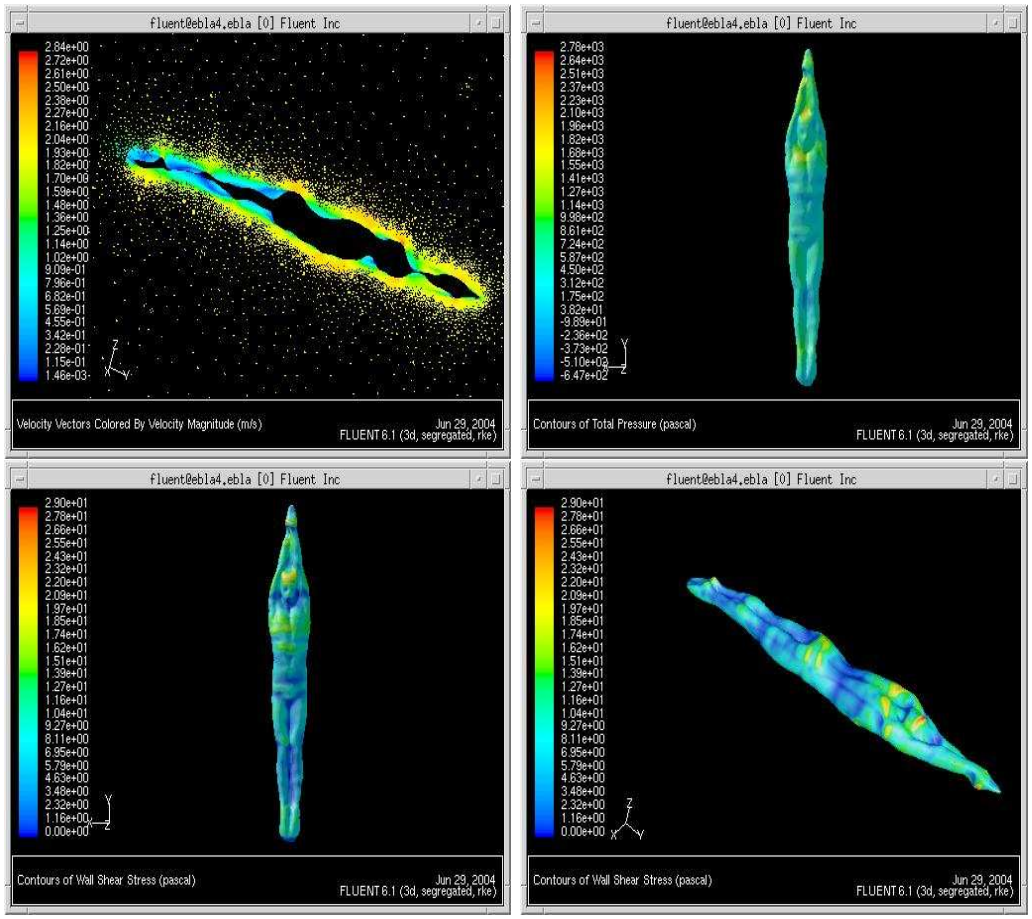

Figure 10: Numerical results for the mesh without holes. Top, Left: Velocity field. Top, Right: Total Pressure. Bottom, Left: Wall Shear Stress on the front. Bottom, Right: Wall Shear Stress on the back.

2.3 Numerical Simulations

In this Section we consider specifically numerical results obtained with the fine mesh in the case of a geometry with holes, since it is needed for having realistic drag and lift numerical results, as we have pointed out in the previous Section. We start with some modeling considerations about the mathematical description of swimsuit roughness. In Tab. 4 we report the results obtained with a condition including a *roughness* parameter $\Delta B = 0.45mm$.

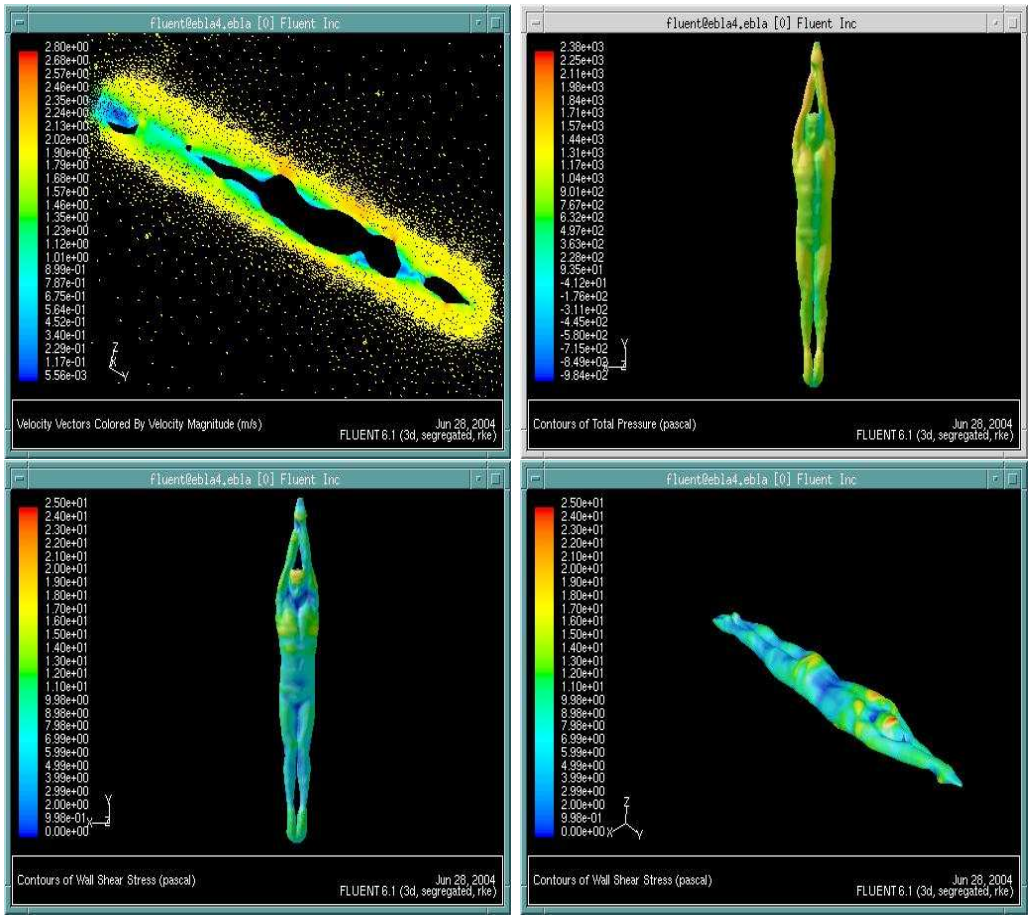

Figure 11: Numerical results for the mesh with holes. Top, Left: Velocity field. Top, Right: Total Pressure. Bottom, Left: Wall Shear Stress on the front. Bottom, Right: Wall Shear Stress on the back.

Roughness is a parameter that can be introduced in FLUENT for a synthetic specification of wall features (for more details, see [10]). The value selected correspond to a roughness inside the viscous sublayer (which is expected to be of the order of a half millimiter). We compare agin the results obtained for the geometries without and with the holes for the case with rough walls. We conclude that also in this case the holes are actually needed for a correct computation of the lift and drag on the swimmer.

The relevant point, however, is that the comparison between the smooth

and the rough cases show that a smooth swimsuit should be better, as it is evident by comparing Tab. 3 and 4. These results give indications opposite to the experimental results obtained in [13]. It is worth pointing out that our results are reasonable, since the roughness modelling available in Fluent is uniform in all the directions. In other terms, a riblet effect is not accounted in standard modules of Fluent. a more precise determination of the roughness effect from the micro to the macro scales is needed and experimental results for the fine tuning of the parameters, as well. This is a crucial point for having realistic numerical simulations at a quantitative level.

In Fig. 12 we show numerical results referred to the case of a geometry with holes with the fine mesh NORM.

The relevant point of these results, even if only at a qualitative level, since we do not have a precise estimate of the roughness parameter, is that the high shear zones can be clearly identified. These zones are in particular the thorax and the legs, around the knees. These results are therefore in perfect agreement with the design of PowerSkin Xtreme©, where a special tissue has been applied in these zones. These results confirm what we have obtained earlier in [12] on the coarse geometry, even if in the present case wall shear stress maps are more irregular for the presence of a more refined geometry, accounting for the specific asymmetric features of the reconstructed body.

Similar results are obtained when considering different inlet velocities. In particular, in Tab. 5 we illustrate the results obtained for inlet velocities of 1.8 m/s, 2 (the value considered above) and 2.2 m/s. Our results show that, as expected, the drag is proportional to the inlet velocity.

Conclusions Numerical simulations carried out in this part of the Project have essentially the role of giving qualitative indications of the drag and stress regions on the swimmer body. Actually, they have provided a scientific justification of some design choices in the development of PowerSkin Xtreme. The legs and the knees are, actually, critical zones where a particular attention should be devoted for reducing the drag, as it has been done for the new swimsuit. In order to carry out significant numerical simulations also at a quantitative level, further work is needed for the correct tuning of the parameters and modeling of the roughness effects induced by the fibers. Therefore, a possible continuation of the project would include, starting from the geometry developed here:

a - a more extensive numerical analysis, coordinated with the group of

	Without Holes	Holes
CPU Time	18h	23h
$h_{swimmer}$	0.005	0.005
h_{layer}	0.02	0.02
h_{ext}	0.5	0.5
N_{elem}	1333018	1344890
$\|\|\mathbf{u}\|\|$ [m/s]	0→2.6115	0→2.6119
u_y [m/s]	-2.57→0.55	-2.58→0.56
wss [Pa]	0→55.41	0→51.91
p_{sta} [Pa]	-2350.2→2190.7	-2362.8→2120.4
p_{dyn} [Pa]	0.08→3408.2	0.34 →3400.3
p_{tot} [Pa]	-326.2→2383	-820.0→2309.7
F_x [N]	-2.07	-2.04
F_y [N] **(drag)**	-58.06	-61.34
F_z [N] **(lift)**	16.74	8.34

Table 4: Numerical results for the geometries without and with holes on a mesh with similar features. Comparison of the results in the case of a rough wall. Rugosity parameter $\Delta B = 0.45mm$.

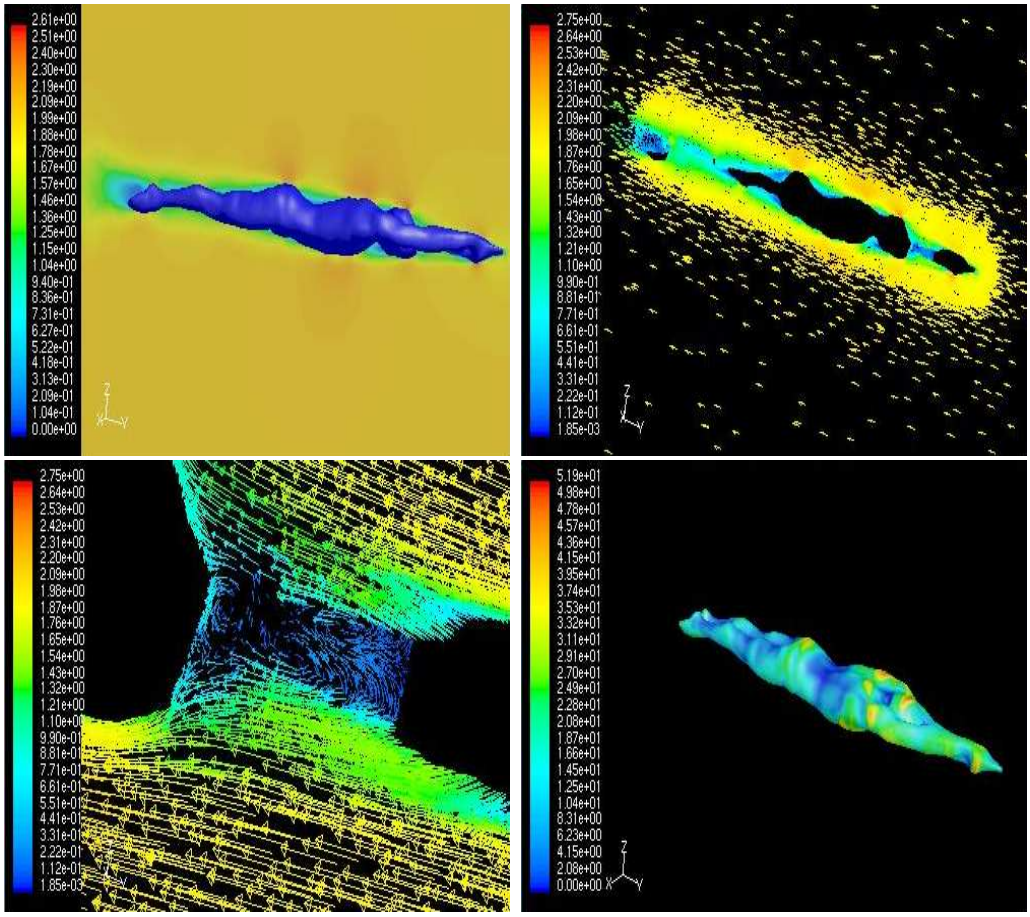

Figure 12: Numerical results for a rough swimsuit. Top, Left: velocity absolute value, Top, Right: Velocity Field. Bottom, Left: Detail of the velocity vector in the hole between the arms. Bottom, Right, wall shear stress.

Redha Tajar, for a cross validation with experimental measures; this could allow an accurate parameters specification; accurate geometrical reconstruction of the swimmer is mandatory for this task;

b - numerical simulation of the heterogeneous swimsuit in order to define the effects of the different rugosity of the tissues.

For the item (b), we carried out some preliminar simulations on the coarse geometry for the sake of simplicity. The results are illustrated in Fig. 13

	1.8 m/s	2.0 m/s	2.2 m/s
F_x **(lift)** [N]	-3.26	-4.05	-4.91
F_y **(drag)** [N]	-39.51	-48.58	-58.56
F_z [N]	6.29	7.75	9.31
vel_{magn} [m/s]	$0.00 \rightarrow 2.24$	$0.00 \rightarrow 2.69$	$0.00 \rightarrow 2.96$
vel_y [m/s]	$-2.39 \rightarrow 0.42$	$-2.66 \rightarrow 0.47$	$-2.93 \rightarrow 0.51$
wss_{magn} [Pa]	$0.00 \rightarrow 20.47$	$0.00 \rightarrow 24.95$	$0.00 \rightarrow 29.83$

Table 5: Numerical results for the geometry with holes on a smooth swimsuit for different inlet velocities.

These preliminar numerical results, in which we have supposed that the special tissue (red and gray) is smoother than the other one (green) show that actually heterogeneous swimsuits could induce a reduction and a more unoiform distribution of the stresses map. Also in this case, a more accurate numerical investigation in this direction should be performed by exploiting a precise quantitative definition of the roughness models and parameters.

3 Microscopic simulations

The second part of the project was devoted to a microscopic analysis of the water dynamics in the viscous sublayer around the tissue fibers. The main goal of this Task was to verify if a riblets effect induced by the fibers is possible and, in particular, if the choice of heterogeneous fibers in the PowerSkin Xtreme could induce a drag reduction with respect to the earlier PowerSkin.

In the earlier part of the Project (see [12]) we faced this part by using a C++ code devloped by MOX. However, we realized during the second part that a strong interaction between the Microscopic and Macroscopic perspectives is mandatory for an accurate analysis at the scale of the swimmer. We decided therefore to proceed by using the same code (FLUENT) in order to have immediatley comparable results. The flow chart of the steps carried out

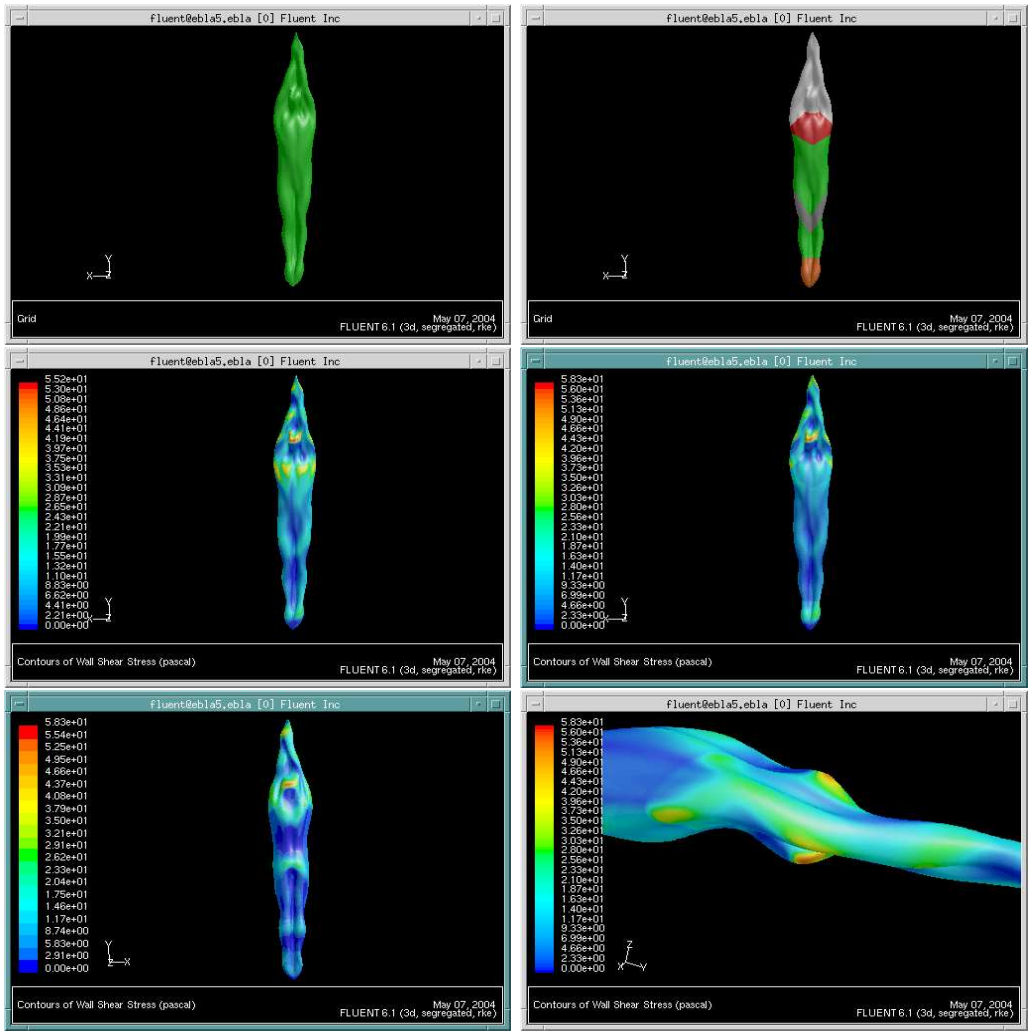

Figure 13: Simulation with a heterogeneous swimsuit. Top, left: Grid for the case with a uniform swimsuit. Top right: Grid for the heterogeneous swimsuit. Center, left: wall shear stress in the uniform swimsuit case; Centr right: wall shear stress for the hetorgeneous swimsuit. Bottom: wall shear stresses for the heterogeneous case from different perspectives. The roughness values are: $\Delta B_{uniform} = 0.4mm$, $\Delta B_{skin} = 0.45mm$, $\Delta B_{green} = 0.1mm$, $\Delta B_{red,gray} = 0mm$.

is illustrated in Fig. 14.

In [12] we presented a code for the automatic generation of the fibers geometry. It was been developed for an easy handling of different geometries and fibers stretching. This code has been used for generating computational meshes of the water flowing around the fibers both for the PowerSkin© and the PowerSkin Xtreme© swimsuits. In the second part of the Project we carried out several numerical simulations for the two tissues. In this Section we illustrate and comment these numerical results, after a short introduction to the riblets effect.

3.1 Riblets effect

The first observations that grooved surfaces are present on the skin of some fishes and this produces a lower drag than for a smooth skin date 1969 (Burdak, Zoologichevisky Zhurnal, in Russian, vol. 48, pp. 1053-1055). Since these observations, many researches have been devoted to this topic. Grooved coating have been experimented upon as drag reduction devices on commercial aircrafts. In the context of sport, riblets have been used at the Los Angeles Olympic Games, 1984, by the US men's rowing boat and in 1987 during the America's Cup by *Stars and Stripes*. A theoretical understanding of the riblets action is however not completely formed. "Riblets seem to work as longitudinal fences to reduce the skin-friction drag by impeding the spanwise movement of longitudinal vortices during the sweep events. In a sense, riblets reduce the skin-friction drag of the turbulent boundary layer by modifying the sequence of near-wall activity by passive spanwise forcing." (from [7]). Following Luchini et al ([1] and [2]) the impedance of cross flow velocity fluctuations in the near-wall region of the boundary layer could be advocated as a drag reduction mechanism. A quantitative characterization of the effectiveness of different groove profiles in retarding secondary cross-flow (see Fig. 15) can be given in terms of the difference between the so called "protrusion heights"). Actually, by asymptotic expansions it is possible to see that the mainstream flow feels the grooved surface as a flat surface at a given depth (*longitudinal protrusion height*) from the riblet tips while the secondary cross-flow feels the surface as a flat one at a different distance (*transversal protrusion height*) which is less than the longitudinal one. The difference between the two protrusion heights seems to drive the effectiveness of the riblets as drag reduction device. As a matter of fact, riblets act in the viscous sublayer, where the flow can be described in terms of (steady) Navier-

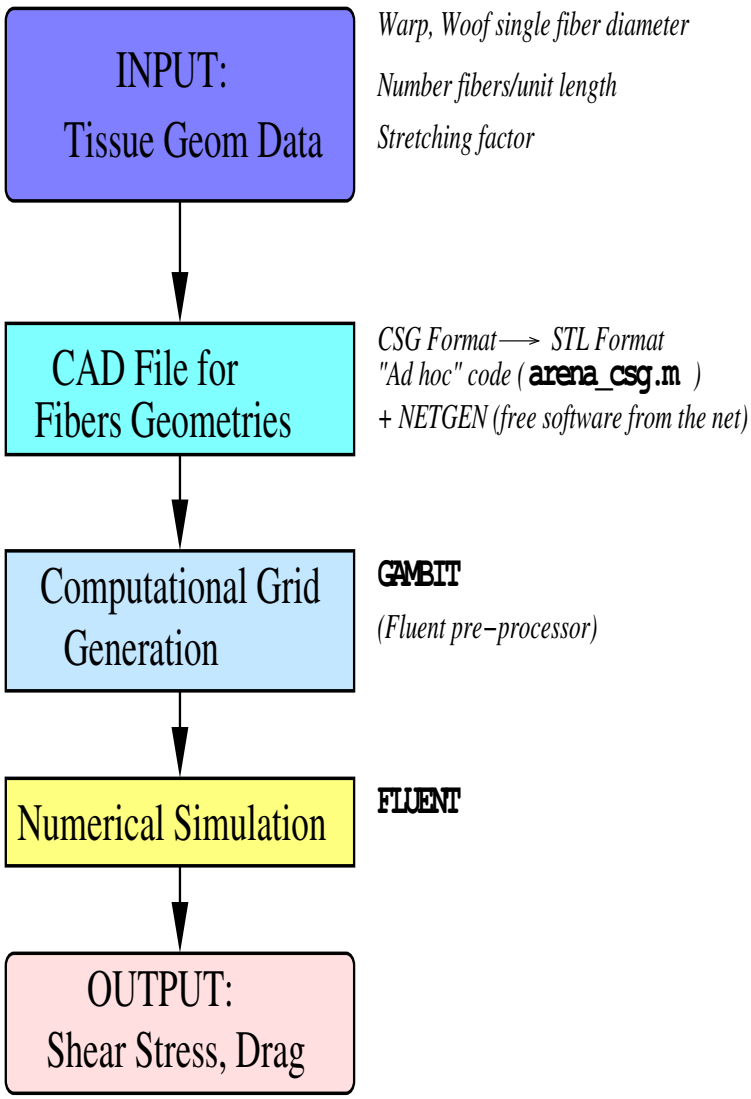

Figure 14: Flow chart of the steps for the *microscopic* simulations.

Stokes equations.

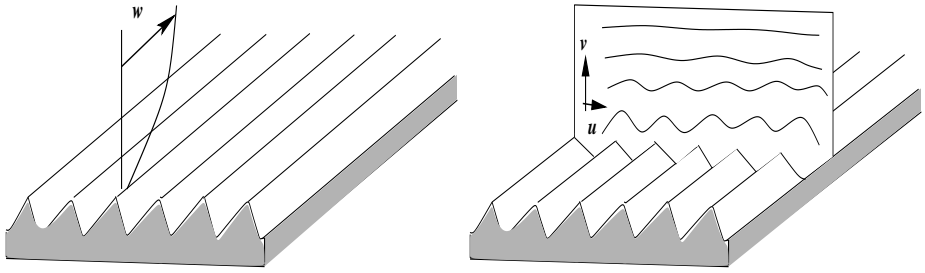

Figure 15: Representation of the water dynamics over a surface featuring riblets following the mainstream (left) and the cross (right) directions. Riblets are supposed to induce a reduction in the transversal motion yielding a drag reduction.

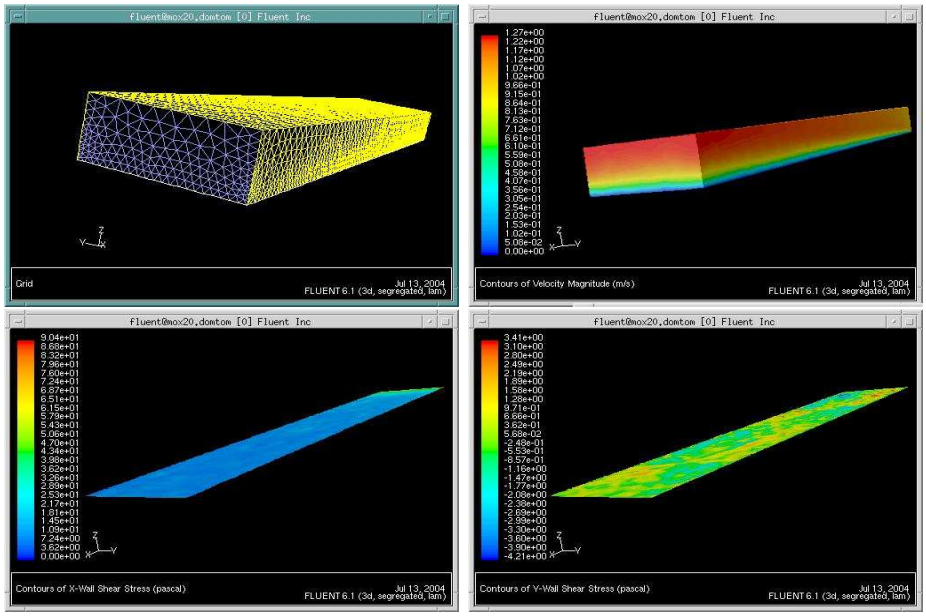

Figure 16: Water simulation over a flat surface. Top, Left: grid. Top, Right: velocity modulus. Bottom, Left: Wall shear stress on the surface along the mainstream. Bottom, Right: Wall shear stress inthe crosswind direction.

In Fig. 16 and 17 we illustrate some numerical results obtained with

Fluent in [14], where the flows over a flat and over a grooved profile are compared. These images have only the aim of illustrating the real reduction in the shear stress (Fig. 16 bottom and 17 bottom), simulated with the same code used in the framework of the present project. Actually, the wall shear stress in the grooved case is reduced both in the transevrsal and in the longitudinal directions.

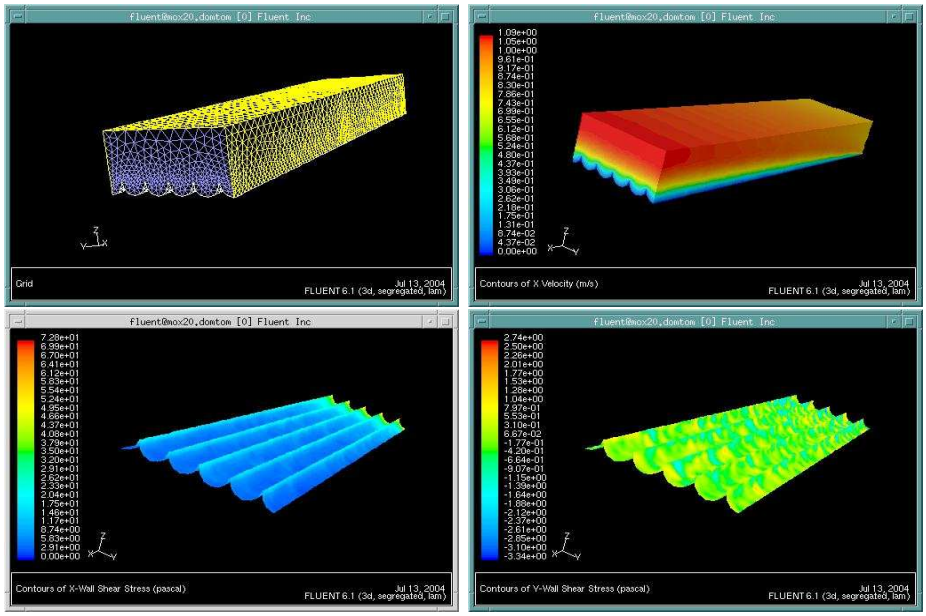

Figure 17: Water simulation over a grooved surface. Top, Left: grid. Top, Right: velocity modulus. Bottom, Left: Wall shear stress on the surface along the mainstream. Bottom, Right: Wall shear stress inthe crosswind direction.

3.2 Generation of the computational domain

We have developed two geometries using the code `arena-csg.m` developed within the Project and the free software `NetGen`. The two geometries refer to the two swimsuits, PowerSkin and PowerSkinXtreme respectively. The output of NetGen has been a file in the `stl` format, which is compatible with the Fluent mesh generator `Gambit`. In particular:

PowerSkin - warp and woof fibers have 0.15 mm diameter;

- two warp fibers have a distance of 0.125 mm; two woop fibers have a distance of 0.159 mm; this distance refer to the rest case, namely a non stretched tissue. Numerical simulations over a stretched tissue can be carried out as well in a possible continuation of the Project.
- the water over the tissue is assumed to have a height of 5 and 10 times the fiber diameter, corresponding to 0.75 mm and 1.50 mm.
- we considered a net of 5 tissue meshes, corresponding to a water box of $1.38mm \times 1.62mm \times 0.75mm(1.50mm)$.

PowerSkinXtreme - warp fibers have $0.30mm$ diameter; woof fibers have $0.18mm$ of diameter.

- two warp fibers have a distance of $0.125mm$; two woop fibers have a distance of $0.159mm$;
- the water over the tissue is assumed to have a height of 5 times the fiber diameter, corresponding to $1.50mm$ and $3mm$;
- we considered a net of 5 tissue meshes, corresponding to a water box of $1.38mm \times 1.62mm \times 0.75mm(3.00mm)$.

The choice of having the height of the computational domain proportional to the largest fibers is motivated by the fact that the viscous sublayer (where we want to simulate the fluid dynamics) is proportional to the riblets tips position.

We carried out several numerical simulations with different boundary conditions.

After the generation of the file for NetGen and the subsequent generation of the stl file, the geometries have been imported in Gambit and the corresponding grids have been generated. In this case we need to simulate the viscous sublayer, where the viscous effects dominate. So we can resort to a pure tetrahedrical grid. We adopted a mesh spacing of $0.05mm$ on the tissue and $0.2mm$ on the upper bound of the water domain. The tetrahedral elements along the z axis (perpendicular to the tissue) are distributed in 20 layers with a growing ratio of 1.12.

The computational domain has been therefore bounded by the follwoing surfaces:

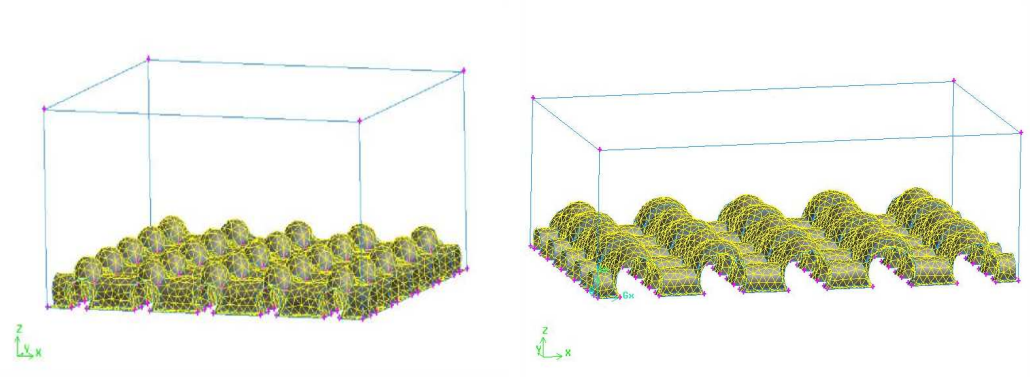

Figure 18: Computational domains for micro-simulations in the viscous sublayer. On the left PowerSkin©. On the right PowerSkin Xtreme©.

1. WALL corresponding to the tissue fibers; at this level, a condition on the velocity has been imposed, namely

$$\mathbf{u} = \mathbf{0}$$

   where $\mathbf{u}$ is the velocity field. A non null velocity field could simulate the absorption of water by the tissue, which could be an interesting test case for a future development of the Project.

2. INLET and OUTLET which are the sections of the water domain perpendicular to the mainstream direction of the water. A periodic condition has been prescribed here, which wants to mimic the repetition of the tissue structure along the mainstream direction. With this condition the incoming flow rate and the coincidence of the velocity and pressure fields on the two boundaries is forced, allowing for the simulation of a completely developed flow;

3. UP and SIDES corresponding to the upper and the lateral boundaries of the computational domain (lateral means in this case that they are parallel to the mainstream) with a "symmetry" condition, forcing null normal stresses.

3.3 Numerical simulations

Following [1], since in the viscous sublayer the motion can be considered dominated by the viscous effect and steady, we simulated a fully developed laminar regime with a costant incoming flow rate of $640kg/(sm^2)$. This incoming flow rate has been tuned in order to have a velocity of about 1 m/s on the external surface of the computational domain, corresponding to one half of the far field velocity (2 m/s). When considering PowerSkin Xtreme, we simulated both the case in which the warp fibers (the largest ones) are oriented along the mainstream (the correct case) and the case with warp fibers perpendicular to the mainstream. From now on, for the sake of brevity, we will denote with PS1 the simulations on the geometry of PowerSkin, with PS2-y the simulations for the PowerSkin Xtreme in the "correct" case and with PS-x the ones for PowerSkin Xtreme with the wrong orientation.

We have in particular analyzed the wall shear stresses and the drag resistance over the swimsuit surface. In particular, we report in Tab 6 and 7 the results obtained for the case with height 5 times the warp fiber diameter (that means $1.5mm$ in the case of PowerSkin Xtreme and $0.75mm$ for PowerSkin) and 10 times ($3mm$ and $1.5mm$) respectively. To make comparable the results obtained in the two cases we consider in particular the drag divided by the area of actually covered by the swimsuits (last row in the two Tables).

In both the cases we observe that even the absolute value of the drag is reduced for a water domain 10 times the warp fibers high, there is an almost constant ratio of *the drag reduction between the PowerSkin Xtreme and the PowerSkin of about 0.4*. These results suggest that the use of the new tissue actually induce a significan drag reduction, in qualitative agreement with the results obtained in [13].

There are however many issues to be clarified, to which further attention should be devoted. In particular:

1. the ratio between the two cases seems very high: at which extent it is affected by the boundary conditions? More numerical simulations and experimental validations should be carried out in order to have a realistic computation at a quantitative level.

2. why PowerSkin Xtreme in the wrong case performs better than PowerSkin? Actually, we would expected that in the uncorret case PowerSkin Xtreme exhibit higher drag than PowerSkin. A possible explanation is

	PS2-y	**PS2-x**	**PS1**
$Q[10^{-3}kg/s]$	2.34	1.39	0.83
$A_{inlet}[10^{-6}m^2]$	2.17	2.17	1.3
$A_{tissue}[10^{-6}m^2]$	7.99	7.99	6.68
$A_{tissue,eff}[10^{-6}m^2]$	3.93	3.93	2.98
$\mathbf{u}_{up}[m/s]$	0.98 $\rightarrow$ 0.99	0.99 $\rightarrow$ 1.021	1.000 $\rightarrow$ 1.056
$\|\|\mathbf{u}\|\|[m/s]$	0 $\rightarrow$ 0.99	0 $\rightarrow$ 1.021	0 $\rightarrow$ 1.056
$u_y[m/s]$	-0.001 $\rightarrow$ 0.99	-0.0127 $\rightarrow$ 1.021	-0.0162 $\rightarrow$ 1.056
$u_x[m/s]$	-0.021 $\rightarrow$ 0.018	-0.020$\rightarrow$ 0.024	-0.038$\rightarrow$ 0.034
$u_z[m/s]$	-0.013 $\rightarrow$ 0.020	-0.017$\rightarrow$ 0.026	-0.026$\rightarrow$ 0.036
$\|\|WSS\|\|[Pa]$	0 $\rightarrow$ 8.60	0 $\rightarrow$ 10.34	0 $\rightarrow$ 26.29
$Drag[10^{-5}N]$ (p+v=tot)	0.26+0.93 = 1.1856	0.656+0.714=1.370	1.122+1.284=2.406
$Drag/A_{tissue,eff}[N/m^2]$	3.03	3.48	8.1

Table 6: Numerical results for the case in which the height of the computational domain is 5 times the largest fiber.

	PS2-y	**PS2-x**	**PS1**
$Q[10^{-3}kg/s]$	4.81	2.84	1.73
$A_{inlet}[10^{-6}m^2]$	7.51	4.43	2.68
$A_{tissue}[10^{-6}m^2]$	7.99	7.99	6.68
$A_{tissue,eff}[10^{-6}m^2]$	3.93	3.93	2.98
$\mathbf{u}_{up}[m/s]$	0.93 $\rightarrow$ 0.96	0.92 $\rightarrow$ 0.922	0.96 $\rightarrow$ 0.97
$\|\|\mathbf{u}\|\|[m/s]$	0 $\rightarrow$ 0.96	0 $\rightarrow$ 0.92	0 $\rightarrow$ 0.97
$u_y[m/s]$	-0.0005 $\rightarrow$ 0.96	-0.008 $\rightarrow$ 0.92	-0.005 $\rightarrow$ 0.97
$u_x[m/s]$	-0.009 $\rightarrow$ 0.008	-0.012$\rightarrow$ 0.012	-0.018 $\rightarrow$ 0.018
$u_z[m/s]$	-0.008 $\rightarrow$ 0.01	-0.013$\rightarrow$ 0.016	-0.015 $\rightarrow$0.021
$\|\|WSS\|\|[Pa]$	0 $\rightarrow$ 4.2	0 $\rightarrow$ 5.11	0 $\rightarrow$ 9.68
$Drag[10^{-5}N]$ (p+v=tot)	0.089+0.426= 0.5146	0.268+0.381=0.6496	0.34+0.57=0.91
$Drag/A_{tissue,eff}[N/m^2]$	1.31	1.65	3.05

Table 7: Numerical results for the case in which the height of the computational domain is 10 times the largest fiber.

that the overlapping among the fibers could anyway induce a sort of riblet effect even if the fibers are oriented in the wrong direction. However, further numerical simulations should be carried out in order to verify this hypothesis.

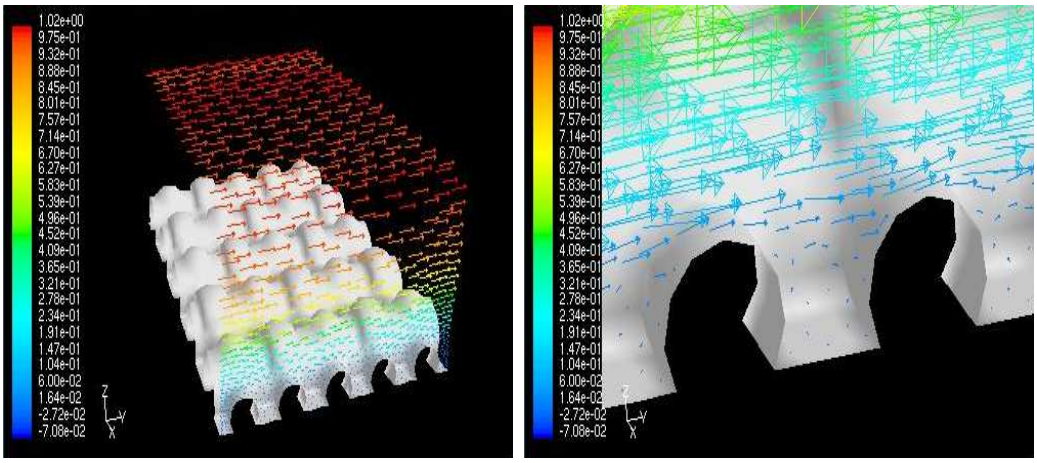

Figure 19: Numerical simulations at the microscopic level: velocity field.

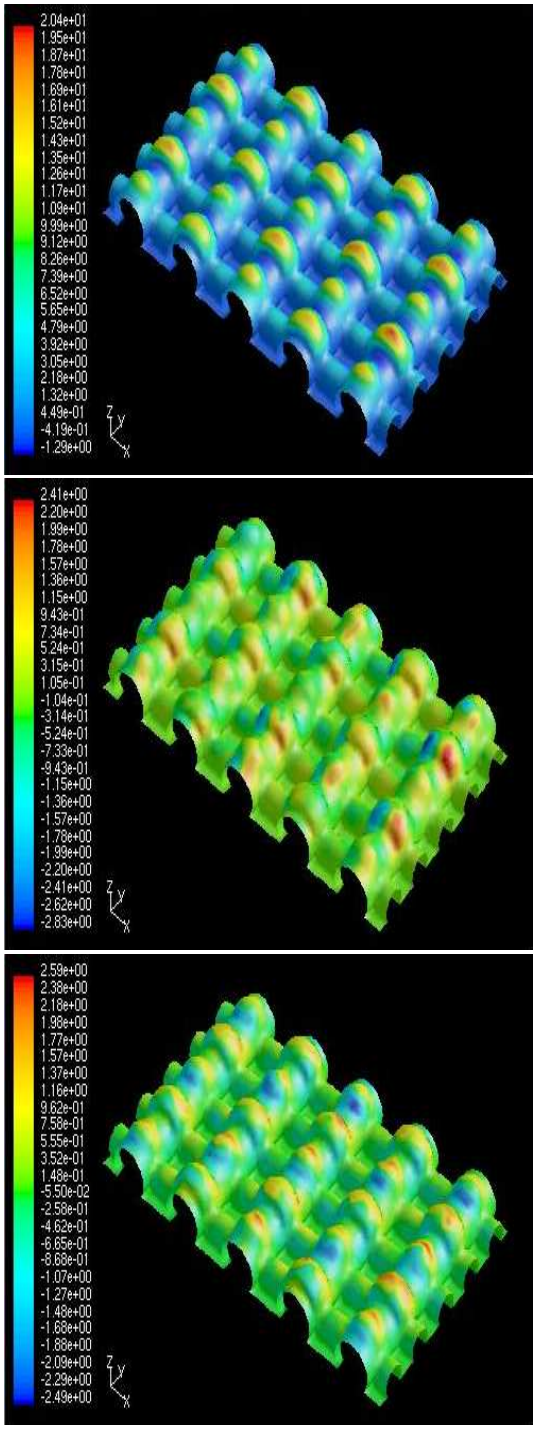

Figure 20: Components of the wall shear stress tensor on PowerSkin Xtreme: along the main stream (top, left), along the crosswind direction (top, right). Along the direction perpendicular to the plane of the tissue (bottom).

4 Conclusions and Future Developments

If we consider the two goals of the Project, we draw the following conclusions.

Advertising The goal of producing good quality and impressive images has been completely reached. During the project the authors have delivered movies and images, materials used in the promotion of the new product. Several interviews and articles on Italian Newspapers and Magazines (Corriere della Sera, Libero, Il Giorno, Il Cittadino di Lodi, GQ) have been dedicated to Arena and the scientific cooperation with MOX during the last Olympic Games. The authors of the present report have presented and will present this research (without any specific details) in different contexts (presentation of the PowerSkin Xtreme swimsuit, June 2004, Fluent User Group Meeting, October 2004, Conference in Piacenza "Mercoledì della Scienza", October 2004).

Water Dynamics Investigations In the Technical Annex to the Project (see [11]) we pointed out the highly innovative taste of the present research and the consequent difficulties. Actually, in the development of the Project, the main difficulties have been:

1. accurate geometrical reconstruction of the swimmer body;
2. determination of parameters and conditions to be specified in the numerical simulations.

Nevertheless, at a qualitative level, we can state that the goals of the Project have been reached.

Macro-scale A real swimmer body has been simulated. The water domain around the body has been accurately meshed; the water dynamics has been simulated and shear stresses on the body has been computed and analyzed. High shear stress zones have been identified.

Micro-scale Computational domains corresponding to the different fibers of Arena swimsuits have been constructed and simulated. The water dynamics around the fibers have been simulated and the results have been analyzed and compared.

In both the cases, at a qualitative level there is good agreement between numerical simulations and measurements obtained in [13].

Arena and its Competitors During the development of the Project, one of the main competitors of Arena©, Speedo©has announced the use of numerical simulations for the development of their new swimsuit. We would like to state the differences of the approaches pursued by Speedo©and by ourselves as far as it is possible to understand from available data about Speedo research.

1. Macroscopic level: at the scale of a swimmer a dummy has been virtually constructed by Speedo. In particular a glass sculpture has been built (recent Hollywood movies like "Spider Man" are quoted as a source of this part of their Project) and accuratelly scanned. Then it has been reconstructed for numerical simulations. The simulations obtained have been a posteriori overlapped to the body of Michael Phelps. Numerical results were mainly devoted to understand the high stress zones on the swimmer body, as for our Project.

   For what concerns the advertising, using the body of a real swimmer, as we have done, should be more effective. Nevertheless, working with a dummy allows to have a very rich and accurate data set for the geometrical reconstruction of the swimmer body.

2. Microscopic level: Strangely enough, this level of analysis is completely absent in the Speedo research. We however think that this is crucial for a real and deep understanding of water dynamics over the fibers (or possibly appendages like the ones of new Speedo swimsuits on the thorax and the shoulders) and for thier mathematical modeling at the swimmer scale.

Future Developments Many issues are still open and could be the subject for a continuation of the Project. More precisely, we list the following ones.

- One of the main goal of a new Project should be the fine and accurate mathematical modeling of the roughness of the tissue at the swimmer scale. To this aim we need to carry out accurate numerical simulations at the microscopic level. In particular extensive experimental validation of the microscopic modelling should be pursued for the quantitative assessment of numerical simulations.

- Experimental validation should be carried out also at the level of the swimmer scale, in order to have precise numerical simulations for supporting the design of new products.

Moreover, further guidelines for new a research could be:

1. improvement of microscopic modeling, accounting for a possible permeability of the tissue and the presence of air bubbles, which could play a relevant role in the drag reduction;

2. simulations of different swimmer positions, for a more complete analysis of critical stresses zones.

References

[1] P. Luchini, F. Manzo, A. Pozzi, *Resistance of a grooved channel to parallel flow and Cross-flow*, J Fluid Mech (1991), vol. 228, pp. 87-108

[2] P. Luchini, *Asymptotic Analysis of Laminar Bloundary Layer Flow Over Finely Grooved Surfaces*, Eur. J. Mech., B/Fluids (1995), vol. 2, pp. 169-195

[3] B. Mohammadi, O. Pironneau, *Analysis of the $k-\epsilon$ Turbulence Model*, Masson, Paris, 1993

[4] A. Quarteroni, A. Valli, *Numerical Approximation of Partial Differential Equations*, Springer-Verlag, New York, 1996

[5] Y. Amirat, J. Simon, *Riblets and Drag Minimization*, in *Optimization Methods in Partial Differential Equations*, American Mathematical Society, ConM 209, pp. 9-17

[6] J. Schöberl, *NetGen 4.3 Handbook*, `http://www.hpfem.jku.at/netgen`

[7] G.E. Karniadakis, *Mechanisms of transverse motions in turbulent wall flows*, Ann. Rev. Fl. Mech., (2003), vol. 35, pp.45-62

[8] M. Cadrens, Drag, Boundary-Layer and Roughness Characteristic of Marine Surface Coated with Anti-Foulings, PhD Thesis, Univ. of Newcastle-Upon-Tyne, 2001.

[9] `www.speedo.com`

[10] Fluent Users' Guide.

[11] A. Veneziani, Technical Annex to the Contract NUMERICAL ASSESSMENT OF PERFORMANCES OF SWIMSUITS, Arena,MOX, November 2003.

[12] E. Foa, A. Veneziani, MID TERM REPORT OF THE PROJECT: "NUMERICAL ASSESSMENT OF PERFORMANCES OF SWIMSUITS", Arena,MOX, May 2004.

[13] R. Tajar, *Analysis Avril 2004*, Report of Cooperation Project with Arena

[14] F. Scalise, *Tecniche di riduzione della resistenza allo scorrimento in regime turbolento mediante riblets*, Tesi di Laurea (primo livello) in Ingegneria Matematica, AA. 2003/2004, Relatore: A: Veneziani